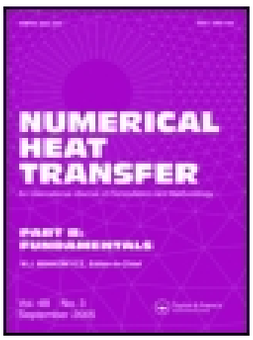

Taylor & Francis
Taylor & Francis Group

Numerical Heat Transfer, Part B: Fundamentals
An International Journal of Computation and Methodology

ISSN: 1040-7790 (Print) 1521-0626 (Online) Journal homepage: http://www.tandfonline.com/loi/unhb20

Nodal integral method for convection-diffusion transport using linear and higher order quadrilateral elements

Rishabh Prakash Sharma & Neeraj Kumar

To cite this article: Rishabh Prakash Sharma & Neeraj Kumar (2018): Nodal integral method for convection-diffusion transport using linear and higher order quadrilateral elements, Numerical Heat Transfer, Part B: Fundamentals, DOI: 10.1080/10407790.2018.1523596

To link to this article: https://doi.org/10.1080/10407790.2018.1523596

NUMERICAL HEAT TRANSFER, PART B
https://doi.org/10.1080/10407790.2018.1523596

Taylor & Francis
Taylor & Francis Group

Nodal integral method for convection-diffusion transport using linear and higher order quadrilateral elements

Rishabh Prakash Sharma[a,b] and Neeraj Kumar[c]

[a]Department of Mechanical Engineering, Thapar University, Patiala, Punjab, India; [b]Department of Energy Science & Engineering, IIT Bombay, Mumbai, India; [c]Department of Mechanical Engineering, Thapar University, Patiala, Punjab, India

ABSTRACT

Generic nodal integral method (NIM) based scheme, utilizing nine noded 2D quadratic elements along with four noded 2D linear elements, is developed to solve the fluid flow and heat transfer equations in complex geometries. Non-linear (quadratic) quadrilateral elements are used for discretization of boundary region and linear quadrilateral elements are used for interior region. Lagrange interpolation functions are used to map both type of elements to corresponding square computational elements. The scheme for Neumann and mixed type of boundary conditions are also developed for quadratic elements. C^1 type continuity condition is imposed at the interfaces of adjacent elements. Numerical results are compared with analytical solutions for diffusion and advection-diffusion equations. Results for Navier–Stokes equations in curved domain are compared with previously reported experimental as well as numerical results. The comparative study has also been done between presently developed scheme using quadratic and linear elements (referred as scheme-1) and scheme based on complete discretization with linear elements (referred as scheme-2). The comparison shows that both the schemes are of nearly second order accurate while the scheme-1 is more accurate than scheme-2. The results show that the efficient mapping of curved surface with quadratic elements improves the accuracy of NIM schemes.

ARTICLE HISTORY
Received 13 June 2018
Accepted 29 August 2018

1. Introduction

Solving the governing equations for fluid flow and heat transfer physics in complex geometries are still a computationally expensive task. Well established numerical methods like finite volume method (FVM) and finite difference method (FDM) still need very fine grids to resolve these physics. Numerical solutions for fluid flow equations in complex geometries are usually obtained by using more refined grids. Thus, a numerical method that can yield better results on a coarse mesh, is desirable.

Nodal integral method (NIM) is one of the nodal methods based scheme [1–9], known for giving accurate numerical results over relatively coarser grids. NIM has established itself as an efficient method to solve the governing equations numerically in regular Cartesian domains (formed by the union of rectangular nodal cells) [3, 7, 9–13]. However, for complex domains, more refinement of these rectangular cells at curved boundaries adversely affects the NIM philosophy of producing quite accurate results using relatively coarse grids [14]. There are also certain limitations

CONTACT Neeraj Kumar neerajkumar@thapar.edu Department of Mechanical Engineering, Thapar University, Patiala, Punjab 147004, USA

Nomenclature

A, B	coefficients in discretized coupling equations for transverse averaged variables in Eqs. (26 and 27) respectively
C^0, C^1	set of zeroth and first order continuous functions respectively
C_i, D_i	i^{th} coefficients of Eq. (4)
f, g	function of space
H	matrix in Eq. (10)
J	Jacobian matrix
k	normal unit vector
K	integration constant in Eqs. (22, 23)
M	matrix in Eq. (9)
m	direction cosines
N	Shape function
P	point in global space $\hat{\zeta}$;
Pe	Peclet number
Q	point in local space ζ
$\mathbb{R}$	real space
Re	Reynolds number
$\bar{S}$	pseudo-source terms
T	temperature
$\bar{T}$	transversed average temperature
u	velocity component in x direction
v	velocity component in y direction
x, y	Cartesian coordinates
α	thermal diffusivity of fluid
$\hat{\zeta}$	spatial domain in (x, y) coordinates
ϕ	general representation of a field variable
θ	angle
ξ, η	local coordinates defining the unit square element
ζ	spatial domain in (ξ, η) coordinates
Subscripts	
i	indices in global x and local ξ directions
j	indices in global y and local η directions
p	point or corner value of field variable in discretized domain
r	radial component of velocity
x, y	first order derivative with respect to x and y respectively
xx, yy	second order derivative with respect to x and y respectively
xy	cross derivative with respect to x and y
θ	angular component of velocity
ξ, η	first order derivative with respect to ξ and η respectively
$\xi\eta$	cross derivative with respect to ξ and η
$\xi\xi, \eta\eta$	second order derivative with respect to ξ and η respectively
Superscripts	
η	η-averaged quantity
ξ	ξ-averaged quantity
$\xi\eta$	cell-averaged quantity

of applicability of this method in the irregular or complex domains due to local transverse integration procedure (TIP) involved in discretization process. TIP is a unique procedure applied in NIM over a local discrete cell to generate cell analytical solution [6]. This procedure requires that the local discrete cell should be fitted in the regular orthogonal coordinate system. These limitations are eased to some extent by developing nodal methods for cylindrical geometries [3, 12, 15] and hexagonal geometries [11].

However, the applicability of NIM in arbitrary-shaped geometries is still limited and only applied to boundary-fitted coordinate geometries [13]. To overcome the above-mentioned limitations, Toreja and Rizwan-Uddin [10] have proposed hybrid methods for fluid flow problems. These hybrid methods, NI-FEM and NI-FAM, are developed by using finite element method (FEM) and finite analytic method (FAM) respectively along with NIM. Although both the hybrid methods are developed to relax the geometry restrictions of computational domains, they are still limited to regular Cartesian grids. Recently this NI-FEM is extended to solve Convection-diffusion equation in three dimensional domain [16]. In this approach the interior of the domain is discretized with regular cuboid elements and curved boundaries are tackled by finite element mesh. NIM methodology is applied for cuboid elements, while the tetrahedral elements are tackled with FEM.

In another approach, Nezami et al. [17] have used arbitrary shaped linear quadrilateral elements for discretization of problem domains. These quadratilateral elements are transformed to square elements using Iso-parametric transformation. NIM scheme using this bi-linear

transformation is further improved by Kumar et al. [8] by including the cross-derivative terms, which were neglected in previous schemes. The scheme for Neumann and other type of boundary conditions is also developed to increase the applicability of these schemes in various physical situations. However, NIM scheme developed by Nezami et al. [17] and Kumar et al. [8], using linear quadrilateral elements to map the arbitrary shaped domain still needs the more number of linear elements at the curved surfaces.

In the current work, NIM scheme is developed using both linear and non-linear quadrilateral elements. Quadratic quadrilateral elements (nine noded) are used to discretized the region of curved boundaries and linear quadrilateral elements (four noded) are used for interior of the domain. Bi-quadratic Lagrange interpolation is used to map the quadratic elements and Bi-linear interpolation is used to map the linear elements into the corresponding local square elements. This approach enhances the flexibility of NIM scheme for its application in complex domain. Moreover, a novel scheme is also developed for implementation of boundary conditions on the curved surfaces.

Developed scheme using the combination of linear and quadratic quadrilateral elements is applied to solve diffusion, advection-diffusion and Navier–Stokes equations in curved domains. For linear problems, numerical results are compared with analytical solutions and for non-linear flow problems (N–S equations) results are compared with previously reported experimental as well as fine grid numerical solutions [18]. The applicability of the NIM scheme for Dirichlet as well as Neumann boundary conditions is also tested in these test cases. The comparative study between the scheme, utilizing linear and quadratic elements with the scheme based on complete linear discretization of problem domain has also been done in this article. This study reveals that the accuracy of the scheme get enhanced without affecting the order of accuracy when quadratic cells are used in discretization of boundary along with linear discretization of interior of domain.

2. Mathematical formulation

2.1. Transformation

The current methodology utilizes linear and quadratic quadrilateral elements to map the arbitrary shaped domain. Each quadratic element has been bijectively mapped using bi-quadratic transformation and each linear element is mapped using bi-linear Lagrangian transformation functions to corresponding square element. For 2D quadratic quadrilateral element there exist three points on each edge of quadratic cell as shown in Figure 1(a). The bijective iso-parametrically transformation from global $\hat{\zeta}$ to local ζ domain $f : \mathbb{R}^2 \rightarrow \mathbb{R}^2$ as follows:

$$P(x, y) = f(Q(\xi, \eta)) \text{where} (x, y) = g(\xi, \eta) \tag{1}$$

where g is a function of (ξ, η). For any continuous function f, $\exists$ a point $\mathbf{Q}(\xi, \eta) \in \zeta$ (local space) for corresponding point $\mathbf{P}(x, y) \in \hat{\zeta}$ (global space), where $\xi, \eta \in [-1, 1]$ and $x, y \in \mathbb{R}$. Two dimensional interpolation function for quadratic element is given in Eq. (2).

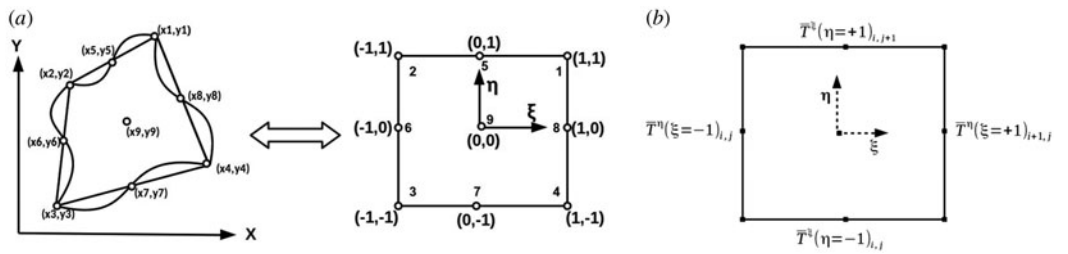

Figure 1. (a) Transformation of 2D quadratic element to square cell (b) Value of transverse averaged variable $\bar{T}$ at cell boundaries.

$$N(\xi_i,\eta_i)=\prod_{i\neq j}^{n=1}\prod_{i\neq k}^{n=1}\frac{(\xi-\xi_j)\cdot(\xi-\xi_{j+1})}{(\xi_i-\xi_j)\cdot(\xi_i-\xi_{j+1})}\cdot\frac{(\eta-\eta_k)\cdot(\eta-\eta_{k+1})}{(\eta_i-\eta_k)\cdot(\eta_i-\eta_{k+1})} \tag{2}$$

here $(\xi_i,\eta_i)\in\zeta$ (local space) and n is number of nodes in a element. Using the above interpolation function, shape function (N_i) can be derived for each node. The iso-parametric transformation between the global and local domain for an element is shown in Eq. (3):

$$\begin{aligned}x&=\sum_{i=1}^{n}N_i.x_i=N_1x_1+N_2x_2+\cdots+N_nx_n\\ y&=\sum_{i=1}^{n}N_i.y_i=N_1y_1+N_2y_2+\cdots+N_ny_n\end{aligned} \tag{3}$$

here $(x_i,y_i)\in\hat{\zeta}$ are the coordinates of ith node. Final set of transformed equations in terms of coefficients is given as in Eq. (4).

$$\begin{aligned}x&=C_1\xi+C_2\eta+C_3\xi^2+C_4\eta^2+C_5\xi\eta+C_6\xi^2\eta+C_7\xi\eta^2+C_8\xi^2\eta^2\\ y&=D_1\xi+D_2\eta+D_3\xi^2+D_4\eta^2+D_5\xi\eta+D_6\xi^2\eta+D_7\xi\eta^2+D_8\xi^2\eta^2\end{aligned} \tag{4}$$

where C_i and D_i are coefficients in terms of x_i and y_i. The detailed expression of these coefficients can be found in standard text of FEM. For a continuous function $\hat{f}(x,y)\in C^0(\hat{\zeta})$ in global space $\exists$ a continuous function $f(\xi,\eta)\in C^0(\zeta)$ in local space as follows:

$$f(\xi,\eta)=\hat{f}\big(x(\xi,\eta),y(\xi,\eta)\big) \tag{5}$$

The corresponding inverse map of this one-one and onto mapping for a continuous function $\hat{f}(x,y)$ is shown as:

$$\hat{f}(x,y)=f\big(\xi(x,y),\eta(x,y)\big) \tag{6}$$

For a second order differentiable function f, the first and second order derivatives of f with respect to x and y are obtained by the chain rule as:

$$\begin{cases}\hat{f}_x=f_\xi.\xi_x+f_\eta.\eta_x\\ \hat{f}_y=f_\xi.\xi_y+f_\eta.\eta_y\end{cases} \tag{7}$$

$$\begin{cases}\hat{f}_{xx}=f_\xi.\xi_{xx}+f_\eta.\eta_{xx}+\xi_x(g_{\xi\xi}.\xi_x+g_{\xi\eta}.\eta_x)+\eta_x\big(f_{\eta\xi}.\xi_x+g_{\eta\eta}.\eta_x\big)\\ \hat{f}_{yy}=f_\xi.\xi_{yy}+f_\eta.\eta_{yy}+\xi_y\big(g_{\xi\xi}.\xi_y+g_{\xi\eta}.\eta_y\big)+\eta_y\big(f_{\eta\xi}.\xi_y+g_{\eta\eta}.\eta_y\big)\\ \hat{f}_{xy}=f_\xi.\xi_{xy}+f_\eta.\eta_{xy}+s_x\big(g_{\xi\xi}.\xi_y+g_{\xi\eta}.\eta_y\big)+\eta_x\big(f_{\eta\xi}.\xi_y+g_{\eta\eta}.\eta_y\big)\end{cases} \tag{8}$$

Transformed PDEs from global to local domain are obtained by utilizing Eqs. (7, 8). These transformed PDEs contains first and second order derivatives like $(\xi_x,\xi_y,\xi_{xx},\xi_{yy}$ etc.) of local coordinate system (ξ,η). The expression for calculating these derivative terms is written as:

$$\mathbf{J}(x,y)=\begin{bmatrix}\xi_x&\xi_y\\ \eta_x&\eta_y\end{bmatrix}=\begin{bmatrix}M_{11}&M_{12}\\ M_{21}&M_{22}\end{bmatrix}^{-1}=\mathbf{M}^{-1} \tag{9}$$

and

$$\begin{bmatrix}\xi_{xx}&\xi_{yy}\\ \eta_{xx}&\eta_{yy}\end{bmatrix}=-2\mathbf{J}(x,y).\begin{bmatrix}H_{11}&H_{12}\\ H_{21}&H_{22}\end{bmatrix}=-2\mathbf{J}.\mathbf{H} \tag{10}$$

The detailed derivation of the Eqs. (9 and 10) are given in appendix-A. **M** and **H** are matrices for first order (Eq. (9)) and second order (Eq. (10)) derivatives respectively. The expression of the elements of both the matrices (**M** and **H**) are also given in appendix-A (Eqs. A.7 and A.8). It should be noted that the elements of Jacobian matrix **J** are non-linear function of local space

(ξ, η) for quadratic cells. However, these elements are linear function of local space for linear quadrilateral cells [17]. Details of the algebraic transformation of a four noded linear element into a square element is given by Nezami et al. [17]. The transformation described in this section allows NIM to map non-linear quadrilateral elements at curved boundary with square computational domains. This results in better approximation of underlying physics at the boundary surface in comparison to the application of linear quadrilateral elements as used by Nezami et al. [17].

2.2. Discretization of domain

In present scheme physical domain is discretized with linear as well as quadratic quadrilateral elements. The quadratic elements are chosen for analogous mapping of curved surfaces while linear elements are used for inner domain as shown in Figure 2(a). It should be noted that quadratic elements with nine nodes of Lagrange family are used for boundaries and four noded linear elements are used for interior of the domain. The application of linear elements in discretization of whole geometry does not fit efficiently at the curved boundaries. In previously reported work [8, 17, 19] the curved surfaces are linearly approximated and enforcement of boundary conditions also done on the linearized surface. Since linearization of curved surface at the boundary does not reflect the true nature of the geometry. Thus the curved boundaries are discretized using quadratic quadrilateral elements which preserve the nature of the geometry in much accurate way.

C^1 type continuity condition, for dependent variables, is enforced at the interfaces of linear-linear and quadratic-linear elements. Application of the C^1 type continuity at the interface of local cells with reference to NIM methodology is described in the following section. The complete discretization of problem domain using quadratic quadrilateral elements is unnecessary since the governing transport equations in fluid flow and heat transfer based on Eulerian frame of reference. In summary, both linear as well as quadratic elements have been used for more accurate discretization.

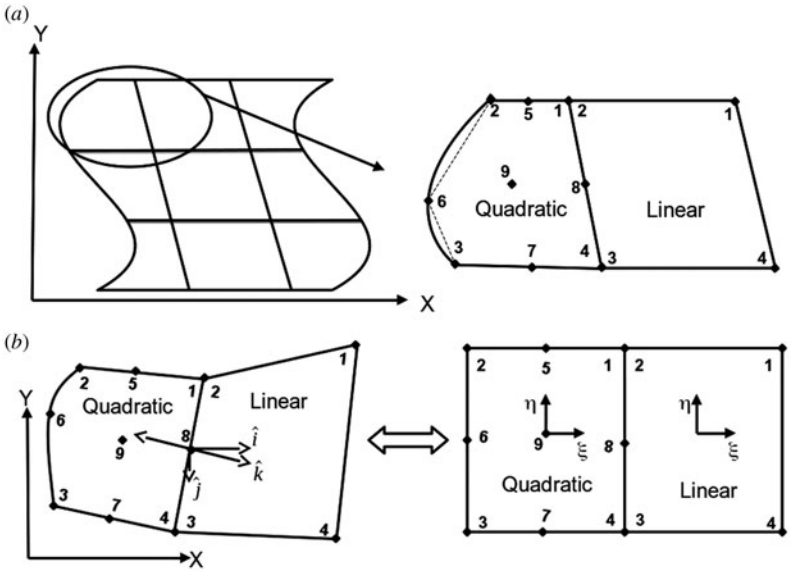

Figure 2. (a) Discretization of arbitrary domain using linear and quadratic elements (b) Mapping of adjacent quadratic and linear elements with corresponding square unit elements.

3. Convection-diffusion equation

The convection diffusion equation is chosen here as a model equation for detailed description of discretization procedure. The generalize form of two dimensional steady state advection diffusion equation in Cartesian coordinate system is:

$$u\frac{\partial \hat{T}}{\partial x}+v\frac{\partial \hat{T}}{\partial y}-\alpha\left(\frac{\partial^2 \hat{T}}{\partial x^2}+\frac{\partial^2 \hat{T}}{\partial x^2}\right)=\hat{f}(x,y) \tag{11}$$

where $\hat{f}(x,y)$ is the source function, α is thermal diffusivity and u, v are velocities in x and y direction respectively. $\hat{T}\in\hat{\xi}$ is temperature distribution in global co-ordinate system. The transformed equation of Eq. (11) in local coordinate system using Eqs. (7, 8) is given as:

$$\begin{aligned}&\left\{\left(\xi_x u+\xi_y v\right)-\alpha\left(\xi_{xx}+\xi_{yy}\right)\right\}\frac{\partial T}{\partial \xi}+\left\{\left(\eta_x u+\eta_y v\right)-\alpha\left(\eta_{xx}+\eta_{yy}\right)\right\}\frac{\partial T}{\partial \eta}\\&-\left\{\alpha\left(\xi_{xx}^2+\xi_{yy}^2\right)\frac{\partial^2 T}{\partial \xi^2}+\alpha\left(\eta_{xx}^2+\eta_{yy}^2\right)\frac{\partial^2 T}{\partial \eta^2}\right\}-2\alpha\left(\xi_x\eta_x+\xi_y\eta_y\right)\frac{\partial^2 T}{\partial \xi\partial \eta}=f(\xi,\eta)\end{aligned} \tag{12}$$

Above-mentioned transformed equation (Eq. 12) is further simplified as follows using the redefinition of terms.

$$u_c\frac{\partial T}{\partial \xi}+v_c\frac{\partial T}{\partial \eta}-\left(\alpha_\xi\frac{\partial^2 T}{\partial \xi^2}+\alpha_\eta\frac{\partial^2 T}{\partial \eta^2}\right)-2\alpha\left(\xi_x\eta_x+\xi_y\eta_y\right)\frac{\partial^2 T}{\partial \xi\partial \eta}=f(\xi,\eta) \tag{13}$$

where

$$\begin{cases}u_c=\left\{\left(\xi_x u+\xi_y v\right)-\alpha\left(\xi_{xx}+\xi_{yy}\right)\right\}\\v_c=\left\{\left(\eta_x u+\eta_y v\right)-\alpha\left(\eta_{xx}+\eta_{yy}\right)\right\}\\\alpha_\xi=\alpha\left(\xi_{xx}^2+\xi_{yy}^2\right)\\\alpha_\eta=\alpha\left(\eta_{xx}^2+\eta_{yy}^2\right)\end{cases}$$

In the above transformed equation (Eq. 13), redefined terms like (u_c, α_ξ etc) depend upon the velocity field, thermo physical properties as well as derivative of local coordinates (ξ_x, ξ_{xx} etc). These derivative terms depend on the type of transformation used for specific element. For quadratic elements, transformation Jacobians are non-linear and for linear elements Jacobians are linear in nature. Thus the redefined terms also depends upon the type of transformation utilized (quadratic or linear elements) for a particular discrete element.

3.1. Transverse integration procedure

The unique procedure of NIM, TIP is applied over transformed Eq. (13). In the Figure 1(b), TIP is applied on the computational domain (ξ,η) using the transverse averaging operators $(1/2)\int_{-1}^{1}d\eta$ and $(1/2)\int_{-1}^{1}d\xi$. These averaging operators generate two transverse averaged ordinary differential equations in ξ and η directions respectively.

$$\bar{u}_c\frac{d\bar{T}^\eta}{d\xi}-\bar{\alpha}_\xi\frac{d^2\bar{T}^\eta}{d\xi^2}=\bar{S}_1^\eta \tag{14}$$

$$\bar{v}_c\frac{d\bar{T}^\xi}{d\eta}-\bar{\alpha}_\eta\frac{d^2\bar{T}^\xi}{d\eta^2}=\bar{S}_2^\xi \tag{15}$$

$\bar{S}_{1,0}^\eta$ and $\bar{S}_{2,0}^\xi$ are pseudo source terms. These terms contains non homogeneous terms of transverse averaged equations. Both of the pseudo source terms are approximated by expanding them

in Legendre polynomial and truncated them in lower orders. These kind of approximations are routinely used in NIM [2, 6]. For *zeroth* order truncation both pseudo source terms become constant which result into the second order approximation of scheme for regular Cartesian domains [2, 3, 20]. But this order may not be guaranteed in discretization of domain using non-orthogonal quadrilateral elements. In present scheme the pseudo source terms are truncated to *zeroth* order. Each homogeneous term of Eqs. (14 and 15) is obtained by the approximation, which says that average of products is approximated to the product of averages as shown in Eq. (16).

$$\frac{1}{2}\int_{-1}^{1} u_c \frac{\partial T}{\partial \xi} d\xi \approx \frac{1}{2}\int_{-1}^{1} u_c d\xi . \frac{1}{2}\int_{-1}^{1} \frac{\partial T}{\partial \xi} d\xi \tag{16}$$

The evaluation of terms $\bar{u}_c, \bar{\alpha}_\xi$ in Eq. (14) are approximated as below:

$$\overline{u_c} = \frac{1}{2}\int_{-1}^{1} u_c d\xi \approx \frac{1}{4}\int_{-1}^{1}\int_{-1}^{1} u_c d\xi d\eta = \frac{1}{4}\int_{-1}^{1}\int_{-1}^{1} \left\{ \left(\xi_x u + \xi_y v\right) - \alpha\left(\xi_{xx} + \xi_{yy}\right) \right\} d\xi d\eta \tag{17}$$

$$\bar{\alpha}_\xi = \frac{1}{2}\alpha\int_{-1}^{1} \left(\xi_{xx}^2 + \eta_{xx}^2\right) d\xi \approx \frac{1}{4}\alpha\int_{-1}^{1}\int_{-1}^{1} \left(\xi_{xx}^2 + \eta_{xx}^2\right) d\xi d\eta \tag{18}$$

The right hand sides of Eqs. (17 and 18) were evaluated for linear elements by treating each cell averaged terms separately as given in Eq. (19) by Nezami et al. [17] and Kumar et al. [8].

$$\begin{aligned} \overline{\left(\xi_x u + \xi_y v\right)\bar{\alpha}\left(\xi_{xx} + \xi_{yy}\right)} &= \overline{\xi_x}.u + \overline{\xi_y}.v - \overline{\alpha\xi_{xx}} - \overline{\alpha\xi_{yy}} \\ \overline{\alpha\left(\xi_{xx}^2 + \xi_{yy}^2\right)} &= \overline{\alpha\xi_{xx}^2} + \overline{\alpha\xi_{yy}^2} \end{aligned} \tag{19}$$

For linear elements the Jacobians are linear in nature and thus individual averaging of terms doesn't affect the cell averaging procedure. While the transformation Jacobians are higher order in case of quadratic elements as described in previous section. These higher order Jacobians contain more feature of curved geometries. Thus for quadratic elements, these approximations are obtained by cell averaging the whole term instead of individual in the following manner (Eq. 20).

$$\begin{aligned} \overline{\left(\xi_x u + \xi_y v\right)\bar{\alpha}\left(\xi_{xx} + \xi_{yy}\right)} &= \overline{\xi_x.u + \xi_y.v} - \overline{\alpha\left(\xi_{xx}\xi_{yy}\right)} \\ \overline{\alpha\left(\xi_{xx}^2 + \xi_{yy}^2\right)} &= \overline{\alpha\left(\xi_{xx}^2 + \xi_{yy}^2\right)} \end{aligned} \tag{20}$$

This modification improves the accuracy of overall scheme for quadratic quadrilateral elements. The pseudo source terms of the transverse average ODEs generated after TIP procedure are also cell averaged in the following way.

$$\begin{aligned} \int_{-1}^{1} \bar{S}_1^{\eta}(\xi) d\xi &\approx \bar{S}_1^{\eta\xi} \\ \int_{-1}^{1} \bar{S}_2^{\xi}(\eta) d\eta &\approx \bar{S}_2^{\xi\eta} \end{aligned} \tag{21}$$

The cell averaged equations (Eqs. 14 and 15), obtained after TIP procedure, are coupled to each other, but the truncation of each pseudo-source terms decouples these equations [21]. The cell analytical solutions, generated from the ODEs (Eqs. 14 and 15), contain geometric transformation as well as nature of underlying physics (Advection and Diffusion). The cell analytical solution for Eq. (14) is given as:

If $\bar{u}_c = 0$

$$\bar{T}^{\eta}(\xi) = \frac{\bar{S}_{1(i,j)}^{\eta\xi}}{2\bar{\alpha}_{\xi(i,j)}}\xi^2 + K_1\xi - K_2 \tag{22}$$

If $\bar{u}_c \neq 0$

$$\bar{T}^{\eta}(\xi) = K_3 . \exp\left\{\frac{Peu_{(i,j)}}{2}\,\xi\right\} + \frac{\bar{S}^{\eta\xi}_{1(i,j)}}{\bar{u}_{c(i,j)}}\,\xi + K_4 \tag{23}$$

where $Peu_{(i,j)}$ is cell Peclet number, which is defined as $Peu_{(i,j)} = 2\bar{u}_{c(i,j)}/\bar{\alpha}_{\xi(i,j)}$ and K_i are integral constants. These integral constants are calculated by applying boundary values of $\bar{T}^{\eta}(\xi)$ for each cell as shown in Figure 1(b). It should be noted that the cell Peclet number contains the convection and diffusion terms for a cell. Thus the cell analytical solution has the adaptive ability to adjust the convection and diffusion physics for each cell depending upon the strength of the convection and diffusion terms. Since $\bar{T}^{\eta}(\xi)$ is the transverse averaged temperature rather than point values thus the discrete numerical solution obtained by NIM methodology are in terms of discrete surface averaged values. Hence the temperature of each cell surface is unique. In Eq. (23) exponential term drives the transport phenomenon of advection-diffusion equation over each cell and leads to inherent upwinding. These transcendental cell analytical solutions are the interpolation functions of the field variables in discrete space. Since they are generated from the governing partial differential equations of the physics, they inherit the nature of that physics. Thus, the said interpolations (cell analytical solutions) of dependent variable leads to much accurate NIM scheme with coarser grids in comparison to other contemporary numerical methods. It also allows to calculate the values of dependent variables at any point inside a cell using cell analytical solutions. Similarly the cell analytical solution for η direction $\bar{T}^{\xi}(\eta)$ can be obtained for $(i,j)^{th}$ cell on solving the Eq. (15).

3.2. Continuity and constrain conditions

As discussed in the previous section the cell analytical solutions are valid over individual cells hence the coupling of these solutions between the two neighboring cells are enforced by application of continuity conditions at the interface of cells. The enforced continuity conditions between the cells are C^1 type (Eq. (24)). The first condition of continuity is straight while the second condition (continuity of the derivatives of field variable at the interface of neighboring cells) is applied using Eqs. (7 and 25). Eq. 25 represents the resolution of normal gradients of the field variable at the interfaces into two perpendicular components where m_x and m_y are the direction cosines in x and y direction respectively. For non-orthogonal grids, the orientation of the interface will also involved in enforcement of continuity conditions. Figure 2(b) represents the application of continuity conditions between quadratic and linear cells. Here $\hat{k}$ represents the normal unit vector at interface and $\hat{i}, \hat{j}$ are the unit vectors in x and y direction respectively. However these type of continuity conditions are also valid between the adjacent linear elements. Details of the application of continuity conditions between two linear elements are given in Kumar et al. [8].

$$\begin{cases} \left(\hat{T}^{\eta}_{i,j}\right)_{14} = \left(\hat{T}^{\eta}_{i+1,j}\right)_{23} = \hat{T}_{i,j} \\ \left.\dfrac{d\hat{T}_{i,j}}{dk}\right|_{14} = \left.\dfrac{d\hat{T}_{i,j}}{dk}\right|_{23} \end{cases} \tag{24}$$

$$\frac{d\hat{T}_{i,j}}{dk} = \frac{d\hat{T}_{i,j}}{dx} m_x + \frac{d\hat{T}_{i,j}}{dy} m_y \tag{25}$$

Application of the above-mentioned continuity conditions between the two neighboring cells (Figure 2(b)) leads to a three point scheme as given in Eqs. (26 and 27) for ξ and η direction respectively.

$$A_1.\bar{T}^{\eta}_{(i-1,j)} - (A_1 + A_2).\bar{T}^{\eta}_{(i,j)} + A_2.\bar{T}^{\eta}_{(i+1,j)} = A_3.\bar{S}^{\eta\xi}_{1(i,j)} + A_4.\bar{S}^{\eta\xi}_{1(i+1,j)} - \left(\frac{T_{p(i,j+1)} - T_{p(i,j)}}{2}\right)\left\{(m_x\eta_x + m_y\eta_y)_{i+1,j} - (m_x\eta_x + m_y\eta_y)_{i,j}\right\} \tag{26}$$

$$B_1.\bar{T}^{\xi}_{(i,j-1)} - (B_1 + B_2).\bar{T}^{\xi}_{(i,j)} + B_2.\bar{T}^{\xi}_{(i,j+1)} = B_3.\bar{S}^{\xi\eta}_{2(i,j)} + B_4.\bar{S}^{\xi\eta}_{2(i,j+1)} - \left(\frac{T_{p(i+1,j)} - T_{p(i,j)}}{2}\right)\left\{(m_x\xi_x + m_y\xi_y)_{i,j+1} - (m_x\xi_x + m_y\xi_y)_{i,j}\right\} \tag{27}$$

where A_i and B_i are coefficients of three point schemes and the expanded form of these terms are given in appendix-B (Eq. B.1). T_p is the point value of temperature at the corner of each cell. In NIM methodology the discrete values are the transverse averaged quantity available at the cell surfaces. So the point values are calculated by utilizing all the surface values in neighborhood of that corresponding point. Details of these approximations can be obtained from [8]. These three point schemes contain pseudo source terms $\bar{S}_1$ and $\bar{S}_2$. Thus two more equations are required for closure. These extra equations are generated by application of physically relevant constraint conditions [7, 8]. In the first constraint condition local cell averaging operator $\frac{1}{4}\int_{-1}^{1}\int_{-1}^{1} d\xi d\eta$ is applied over the transformed PDE (Eq. 13). This results a relation between pseudo source terms and actual source term as shown in Eq. (28).

$$\bar{S}^{\eta\xi}_{1(i,j)} + \bar{S}^{\xi\eta}_{2(i,j)} = \bar{f}^{\eta\xi} - \frac{1}{4}\int_{-1}^{+1}\int_{-1}^{+1} 2\alpha\left(\xi_x\eta_x + \xi_y\eta_y\right)T_{\xi\eta}d\xi d\eta \tag{28}$$

Again the right hand side terms of Eq. (28) are approximated in a similar way as described in Eq. (20). The second constraint condition is uniqueness of cell averaged values of dependent variables. Thus the cell averaged value is independent of the order of directional averaging i.e $\bar{T}^{\xi\eta}_{i,j} = \bar{T}^{\eta\xi}_{i,j}$. Final set of discrete equations are generated with the application of these two constraint conditions. The form of the set of final discrete equations is similar to the equations derived by Kumar et al. [8] for linear quadrilateral elements. Thus expanded form of final discrete equations is not given here for sake of brevity.

4. Diffusion and Navier–Stokes equations

The general form of two dimensional Poisson equation or 2D steady state diffusion equation in Cartesian coordinate system, is given by:

$$\nabla^2\hat{T} = \hat{f}(x,y) \tag{29}$$

and the corresponding transformed equation in (ξ,η) local coordinate system is:

$$\left(\xi_{xx} + \xi_{yy}\right)T_\xi + \left(\eta_{xx} + \eta_{yy}\right)T_\eta + \left(\xi^2_{xx} + \xi^2_{yy}\right)T_{\xi\xi} + \left(\eta^2_{xx} + \eta^2_{yy}\right)T_{\eta\eta} + 2\left(\xi_x\eta_x + \xi_y\eta_y\right)T_{\xi\eta} = f(\xi,\eta) \tag{30}$$

Since the transformed diffusion equation is similar to the transformed advection-diffusion equation except the velocity terms appearing in Eq. (12). Thus further procedure for discretization of transformed diffusion equation (Eq. (30) by NIM is similar to the scheme developed for advection-diffusion equation. The detailed development of the scheme for diffusion equations is not shown here for the sake of brevity.

Again scheme for Navier–Stokes equations is developed with reference to the scheme developed for the convection diffusion equation as discussed in previous section. Since N–S equations are non-linear in nature due to the convective terms, these terms are approximated to generate cell analytical solution. Hence the approximations, introduced by taking the cell averaged velocities in the convection terms of N–S equations, are defined as:

$$\bar{u}_{cell(i,j)} = \frac{\bar{u}^{\eta}_{i,j} + \bar{u}^{\eta}_{i+1,j} + \bar{u}^{\xi}_{i,j} + \bar{u}^{\xi}_{i,j+1}}{4} \quad \text{and} \quad \bar{v}_{cell(i,j)} = \frac{\bar{v}^{\eta}_{i,j} + \bar{v}^{\eta}_{i+1,j} + \bar{v}^{\xi}_{i,j} + \bar{v}^{\xi}_{i,j+1}}{4} \tag{31}$$

With reference to the Figure 1(b), the cell average velocities for $(i,j)th$ cell are evaluated by taking the mean of cell surface velocities (Eq. (31)). This approximation is verified and tested in the previously developed schemes for N–S equations by Wang and Rizwan [7] and Kumar et al. [9, 19]. This leads to linear form of convective terms (Eq. 32) in N–S equations similar to the convection diffusion equation valid over the discretized domain (local cell).

$$V.\nabla V \approx V_{cell}.\nabla V \tag{32}$$

Thus the cell analytical solutions for N–S equations are generated for discretized local domain in the same way as convection diffusion equation. The three point scheme for N–S equation will also be similar to the Eqs. (26 and 27). The only difference is the source term which is pressure gradient as well as body force terms. Along with the momentum equations, pressure Poisson equation $(\nabla^2 P = \nabla.V)$ is solved to obtained the divergence free velocity field. Here the pressure Poisson equation is similar to the pressure equation used in SIMPLE algorithm. The pressure and velocity coupling is obtained by utilizing the pressure correction based algorithm proposed by Kumar et al. [9] with reference to the NIM methodology.

5. Boundary conditions enforcement for quadratic elements

In the present scheme the implementation of boundary conditions over a curved surface is done by piecewise linear approximation of the quadratic surface on curved boundary. Dirichlet and Neumann type boundary conditions for linear quadrilateral elements using NIM methodology has been developed by Kumar et al. [8]. Implementation of Dirichlet boundary condition is straightforward. However the implementation of Neumann boundary condition is not trivial on the curved boundary. Thus piecewise linearization is done for quadratic elements on the curved surface as shown in the Figure 3. The Neumann boundary condition is applied on each linear segment of quadratic element. Same cell analytical solution for a quadratic cell is utilized to enforce the Neumann boundary condition over two different linearized surfaces of quadratic element.

$$\frac{\partial \hat{\phi}}{\partial k} = \frac{\partial \hat{\phi}}{\partial x} m_x + \frac{\partial \hat{\phi}}{\partial y} m_y \tag{33}$$

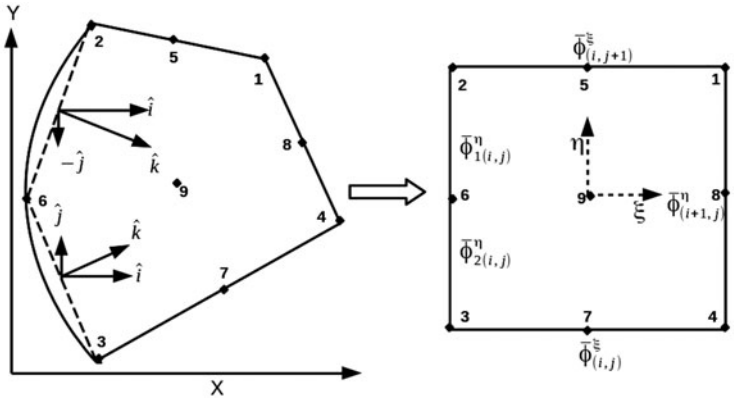

Figure 3. Piecewise linearization of a curved surface of quadratic element.

General form of Neumann boundary condition at a surface for a field variable ϕ can be written as in Eq. (33), where m_x and m_y are direction cosines in x and y direction respectively and $\hat{k}$ is normal unit vector as used in continuity condition. Now on a quadratic edge (2–3) in Figure 3, gradients are calculated over two piecewise linearized surfaces (2–6) and (6–3) as follows:

$$\left.\frac{\partial\hat{\phi}}{\partial k}\right|_{2-6} = \left(\frac{\partial\hat{\phi}}{\partial x}m_x\right)_{2-6} + \left(\frac{\partial\hat{\phi}}{\partial y}m_y\right)_{2-6} \tag{34}$$

$$\left.\frac{\partial\hat{\phi}}{\partial k}\right|_{6-3} = \left(\frac{\partial\hat{\phi}}{\partial x}m_x\right)_{6-3} + \left(\frac{\partial\hat{\phi}}{\partial y}m_y\right)_{6-3} \tag{35}$$

The Eqs. (34 and 35) are transformed into the computational domain (ξ, η). For both the surfaces, the corresponding transformed equations are given as Eqs. (36 and 37):

$$\left.\frac{\partial\hat{\phi}}{\partial k}\right|_{2-6} = \left(\frac{\partial\bar{\phi}^{\eta}}{\partial\xi}\xi_x + \frac{\partial\bar{\phi}^{\eta}}{\partial\eta}\eta_x\right)m_x\Bigg|_{2-6} + \left(\frac{\partial\bar{\phi}^{\eta}}{\partial\xi}\xi_y + \frac{\partial\bar{\phi}^{\eta}}{\partial\eta}\eta_y\right)m_y\Bigg|_{2-6} \tag{36}$$

$$\left.\frac{\partial\hat{\phi}}{\partial k}\right|_{6-3} = \left(\frac{\partial\bar{\phi}^{\eta}}{\partial\xi}\xi_x + \frac{\partial\bar{\phi}^{\eta}}{\partial\eta}\eta_x\right)m_x\Bigg|_{6-3} + \left(\frac{\partial\bar{\phi}^{\eta}}{\partial\xi}\xi_y + \frac{\partial\bar{\phi}^{\eta}}{\partial\eta}\eta_y\right)m_y\Bigg|_{6-3} \tag{37}$$

In the above equations gradients of dependent variable in ξ direction are obtained from the cell analytical solution $\bar{\phi}^{\eta}(\xi)$. However the gradients in η direction are calculated by utilizing the discrete value of the field variable calculated at each node of the cell. Since in NIM methodology the values are available at cell surfaces in terms of transverse averaged values as shown in Figure 3. The point values at the node points of quadrilateral element are calculated by taking mean of the nearest cell surfaces values available to a corresponding point. The details of the evaluation of discrete point values is given by Kumar et al. [8]. Thus in Eqs. (36 and 37) the gradients of dependent variable in η direction are evaluated as given in Eqs. (38 and 39).

$$\left.\frac{\partial\bar{\phi}}{\partial\eta}\right|_{2-6} = \frac{\phi_2 - \phi_6}{\Delta\eta/2} \tag{38}$$

$$\left.\frac{\partial\bar{\phi}}{\partial\eta}\right|_{6-3} = \frac{\phi_6 - \phi_3}{\Delta\eta/2} \tag{39}$$

where $\Delta\eta = 2$ is the size of local cell in η direction. The expression of Neumann boundary condition at each linearized surface (2–6 and 6–3 in Figure 3) contains point value of dependent variable ϕ_6 which is further approximated in terms of connected surface values of field variable $(\bar{\phi}^{\eta})_{2-6}$ and $(\bar{\phi}^{\eta})_{6-3}$ as:

$$\phi_6 = \frac{\bar{\phi}^{\eta}_{2-6} + \bar{\phi}^{\eta}_{6-3}}{2} \tag{40}$$

This leads to the close form implementation of the Neumann boundary condition on the curved surface utilizing quadratic quadrilateral elements. Similarly we can enforce mixed type boundary conditions on quadratic surfaces by careful application of above approximations.

6. Numerical results and discussion

The schemes based on NIM using non-linear and linear quadrilateral elements have been tested for both linear and non-linear governing differential equations. The diffusion and convection-diffusion equations are solved in 2D cylindrical wedge domain and the results are compared with

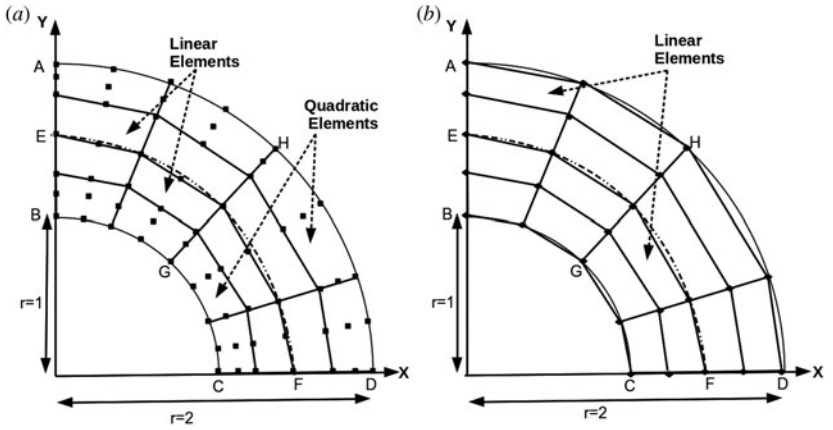

Figure 4. Different discretization scheme used in NIM (a) Scheme-1 (b) Scheme-2.

the analytical solutions. Both Neumann and Dirichlet type of boundary conditions are applied and tested in these cases.

In all the cases, quadratic quadrilateral elements are applied to map the curvature boundary of the physical domain and internal nodal cells are linear quadrilateral elements as shown in Figure 4(a). The above mentioned scheme is also compared with the scheme based on complete linear discretization of whole domain as shown in Figure 4(b). Thus here onwards we will refer discretization using quadratic-linear quadrilateral elements as scheme-1 (Figure 4(a)) and discretization of whole domain using linear quadrilateral elements as scheme-2 (Figure 4(b)). The comparative studies have been done between the results obtained from both type of discretization procedure. Numerical scheme, based on the discretization procedure of scheme-1, is further applied to solve the Navier–Stokes equations in 2D cylindrical wedge domain. Polar lid driven cavity is chosen as a test problem for validation of the numerical results with previously reported numerical and experimental results by Fuchs and Tillmark [18]. This test problem is routinely used to verify the applicability of numerical scheme for the solution of Navier–Stokes equations in curved domains [22–24].

6.1. Test case-1

In this test case Laplace equation $\nabla^2 T = 0$ is numerically solved over a 2D cylindrical wedge domain with wedge boundaries $1 \leq r \leq 2$; $0 \leq \theta \leq \pi/2$ as shown in the Figure 4. The boundary conditions are Dirichlet type at surface AB, CD and AD ($T_{(r,\pi/2)} = T_{(r,0)} = 1$ and $T_{(2,\theta)} = \cos(4\theta)$ respectively) and one Neumann condition $dT/dr|_{(1,\theta)} = 0$ on BC side of the wedge. The applicability of this numerical scheme for Neumann as well as Dirichlet boundary condition is tested in this test problem. Numerical results are compared with analytical solution. The scheme based on NIMs has ability to produce reasonably accurate results on very coarse grid structure [5, 6, 9, 10, 19]. Thus comparative coarse grid structure are chosen to show its effectiveness of developed scheme.

For qualitative comparison, results are compared at central lines EF and GH as shown in Figure 4. Computation is done with different grid sizes. Figure 5(a) and 5(b) show the variation of temperature along the centerlines EF and GH respectively. The discrete temperatures along EF and GH generated by scheme-1 (quadratic-linear quadrilateral elements) and scheme-2 (linear quadrilateral elements) using the mesh sizes $(4 \times 4), (6 \times 6)$, and (8×8) are shown in these plots. Both the schemes are compared with reference to analytical solutions.

It should be noted that both the schemes are close to the analytical solution. This is due to the effectiveness of coarse grid NIM schemes. Still the zoomed comparison (Figure 5(a) and 5(b)) for

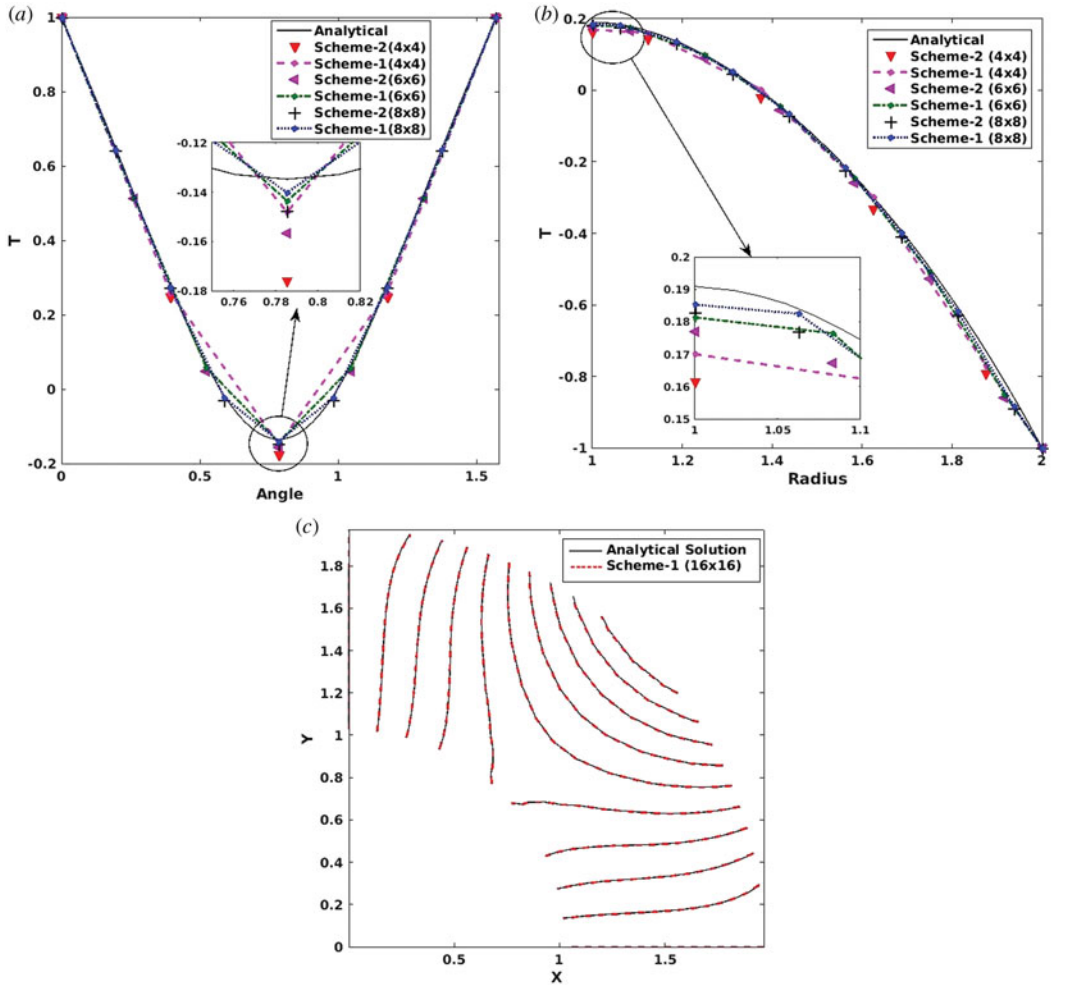

Figure 5. (a) Variation of temperature at r = 1.5 and $0 \leq \theta \leq \pi/2$ (b) at $\theta = \pi/4$ and $1 \leq r \leq 2$ (c) Comparison of contours of temperature of scheme-1 (16×16 grids) with analytical solution.

all the grid sizes at particular location shows that the results obtained from the scheme-1 on similar mesh sizes are closer to analytical solution in comparison to scheme-2. Thus more realistic mapping of curvature boundaries utilizing the quadratic quadrilateral elements (scheme-1), enhances the accuracy of NIM in comparison to scheme-2.

This test case is also utilized to test the implementation of Neumann boundary condition at curved boundaries. The applicability of Neumann boundary condition on curved surface using scheme-1 can be visualized at boundary $r = 1$ in Figure 5(b). It is observed that for all the grid sizes $(4 \times 4), (6 \times 6)$, and (8×8), scheme-1 can tackle Neumann boundary condition in more accurate way in comparison to scheme-2. Thus piecewise linearization of the curved surface using quadratic elements for Neumann boundary conditions plays an effective role in improvement of NIM methodology. Quantitative comparison is also done to observe the behavior of numerical scheme toward quadratic elements.

Table 1 contains L2 norm errors (Rms error) for the whole domain as well as for the boundary surface where the Neumann boundary condition is applied (surface BC, Figure 4). The definition of the L2 norm error is given by Eq. (41).

Table 1. L2 norm error for test case-1 for all grids and for boundary cells.

Mesh	Total L2 norm error		Neumann boundary L2 norm error	
	Scheme-1	Scheme-2	Scheme-1	Scheme-2
4×4	1.3443×10^{-2}	1.8816×10^{-2}	1.0528×10^{-2}	1.8901×10^{-2}
8×8	4.8256×10^{-3}	7.2010×10^{-3}	2.9999×10^{-3}	6.0068×10^{-3}
16×16	1.3030×10^{-3}	2.0331×10^{-3}	7.4564×10^{-4}	1.6661×10^{-3}
32×32	3.3012×10^{-4}	5.3317×10^{-4}	1.8353×10^{-4}	4.3943×10^{-4}

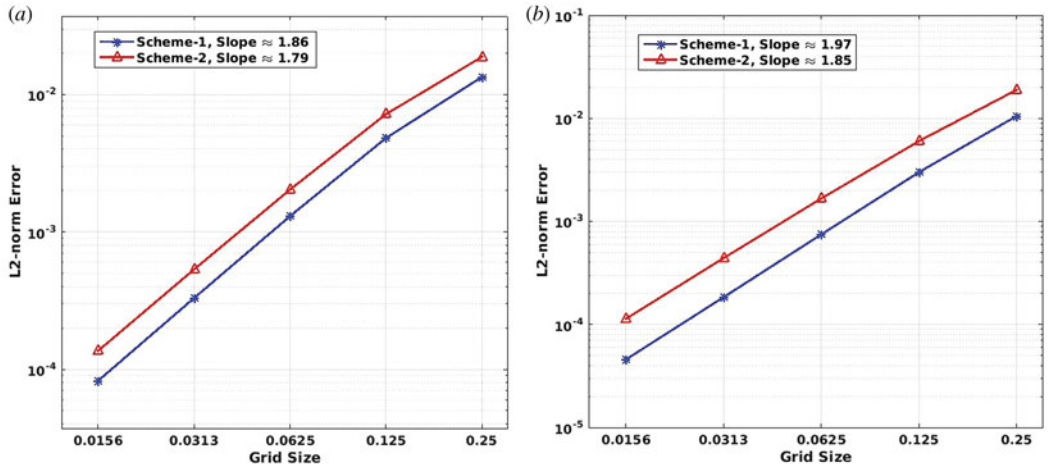

Figure 6. Variation of L2 norm error for diffusion equation for (a) whole domain (b) boundary cells.

$$error = \sqrt{\sum_{1}^{n} \frac{(T_{exact} - T_{numerical})^2}{n}} \tag{41}$$

where n is the number of grid points. Different grid sizes (4×4), (8×8), (16×16), and (32×32) are used to calculate L2 norm errors for both the schemes.

From the Table 1, it is noted that as the grid resolution is reduced by half the reduction factor for L2 norm error, is nearly 2.6-3.9 for both the schemes which leads to nearly second order scheme. This behavior is also visible in Figure 6(a). It should also noted that order of the scheme-1 is slightly improved than scheme-2. However for Neumann boundary (Figure 6(b) and Table 1) the order as well as accuracy of scheme-1 is much better than scheme2. For coarsest grid size (4×4), scheme-1 is nearly 28% more accurate than scheme-2. However at the Neumann boundary, scheme-1 is nearly 44% more accurate than scheme-2. It is also observed from Table 1 that scheme-1 maintains it's accuracy over scheme-2 for all the grid sizes. Thus utilization of quadratic elements for curvature boundaries pays its dividend by increasing the accuracy of the scheme-1 especially at the curved surface without changing the order of the scheme. Figure 5(c), shows the comparison of temperature contours generated by scheme-1 using grid size (16×16) with analytical solution.

6.2. Test case-2

The nodal scheme developed for Convection-diffusion equation is utilized to solve this physics in arbitrary shaped domains. Again the physical domain is cylindrical wedge domain similar to the previous test case as shown in Figure 7. Variation of velocity field is hyperbolic $(u = u_o/r)$ in radial direction and constant in angular direction, where u_o is the mean velocity. Boundary condition for temperature at BC and AD surfaces is zero $(T_{(1,\theta)} = T_{(2,\theta)} = 0)$, inlet temperature at

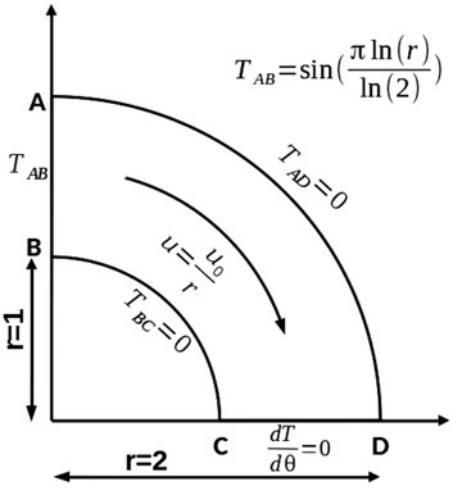

Figure 7. Schematic diagram of advection-diffusion problem in 2D cylindrical wedge.

AB surface is $T_{(r,\pi/2)} = \sin\{\pi \ln(r)/\ln(2)\}$ and at CD surface temperature gradient is zero i.e $dT/d\theta|_{(r,0)} = 0$ as shown in Figure 7.

Both the schemes (scheme-1 and scheme-2) are applied to solve this test problem and the results are compared with analytical solution given in Eq. (42). [25].

$$T(r,\theta) = \sin\frac{\pi \ln r}{\ln 2}\left\{\frac{s_1 \exp\left(s_1\frac{\pi}{2} + s_2\theta\right) - s_2 \exp\left(s_2\frac{\pi}{2} + s_1\theta\right)}{s_1 e^{s_1\frac{\pi}{2}} - s_2 e^{s_2\frac{\pi}{2}}}\right\} \tag{42}$$

where

$$s_{1,2} = \frac{u_0 \pm \sqrt{u_0^2 + \frac{2\pi\alpha}{ln2}}}{2\alpha}$$

The effect of relative strength between the advection and diffusion physics on the scheme is tested in this test case by the application of different Peclet numbers. Thus the Peclet number of Pe =700 (high advection) and 7 (low advection) are chosen to verify the numerical results with analytical solutions. Here, Peclet number is defined for this test domain as $Pe = (2u_o(r_2 - r_1)/\alpha)$, where $u_o = 1$ and α is thermal diffusivity of fluid. The qualitative comparison is done by comparing the temperature variation at surface GH, $\theta = \pi/4$ and $1 \le r \le 2$. Again the grid sizes utilized are $(4 \times 4), (6 \times 6)$ and (8×8). The variation of temperature, along this surface GH using different grid sizes, is shown in Figure 8(a) and 8(b) for both the Peclet numbers 7 and 700 respectively.

In Figure 8, results obtained by both the schemes on same grid sizes are compared with analytical solutions. It should be noted that for both the Peclet numbers, the results obtained by scheme-1 is closer to the exact solutions.

The detailed quantitative comparative study between the scheme-1 and scheme-2 is done for this test case by comparing L2 norm errors. Again the same grid sizes $(4 \times 4), (8 \times 8), (16 \times 16)$, and (32×32) are used for the comparison. L2 norm error for Pe =7 and 700 by scheme-1 and scheme-2 at different grid sizes are in shown in Table 2. For low Peclet number (Pe =7), as the size of grid reduced by half, the reduction factor for both the schemes is nearly 3.9.

However, for high Peclet number (Pe =700), as the grid gets doubled the reduction factor for both the schemes is approximately 3.1–4.2. This leads to a nearly second order numerical scheme for both the Peclet numbers which is also visible in Figure 9. Numerical experiments are also conducted to evaluate the order of accuracy of both the schemes for the physics ranging from

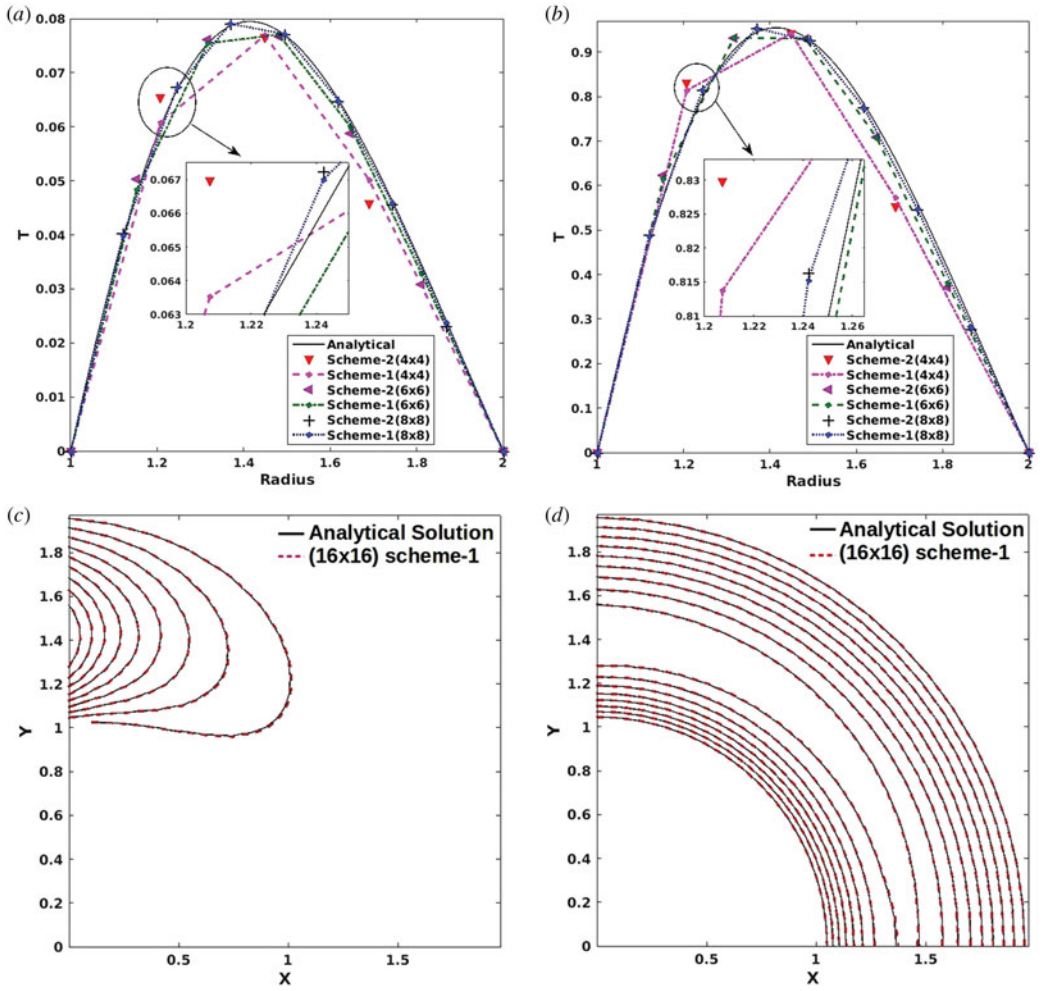

Figure 8. (a) Variation of temperature along GH at $\theta = \pi/4$ and $1 \leq r \leq 2$ at Pe =7 (b) Pe =700 (c) Comparison of isotherms by scheme-1 (16×16 grids) with analytical solution at Pe =7 (d) Pe =700.

Table 2. L2 norm error for different Peclet numbers.

Mesh	L2 norm error at Pe =7		L2 norm error at Pe =700	
	Scheme-1	Scheme-2	Scheme-1	Scheme-2
4×4	1.5608×10^{-2}	1.6531×10^{-2}	2.6671×10^{-2}	3.0437×10^{-2}
8×8	3.9918×10^{-3}	4.4923×10^{-3}	8.6047×10^{-3}	9.5942×10^{-3}
16×16	1.0301×10^{-3}	1.1876×10^{-3}	2.3135×10^{-3}	2.5810×10^{-3}
32×32	2.7198×10^{-4}	3.1463×10^{-4}	5.7201×10^{-4}	6.4790×10^{-4}

diffusion dominant to convection dominant. Thus the order of accuracy is calculated for 0.1 to 700 Peclet numbers as shown in Table 3. From Table 3, it is observed that both the schemes are nearly second order accurate for variety of Peclet numbers. Thus it is concluded that scheme-1 improves the accuracy of NIM for both diffusion as well as convection-diffusion equation over scheme-2 while maintaining the order (second order) of NIM scheme. Figure 8(c) and 8(d) depicts the comparison of isotherms for Pe =7 and Pe =700 respectively generated by scheme-1 using (16×16) grid size with analytical solutions.

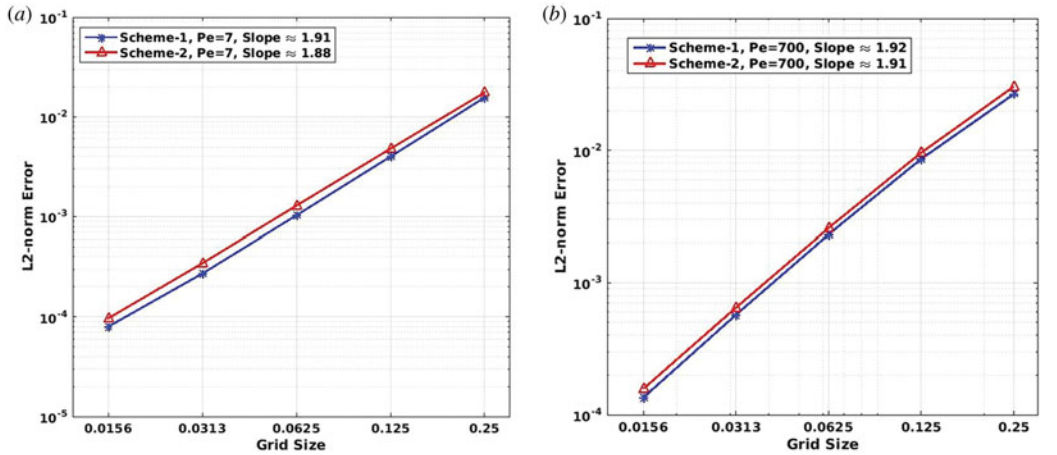

Figure 9. Variation of L2-norm error for convection-diffusion equation at (a) Pe =7 (b) Pe =700.

Table 3. Order of scheme with different Peclet numbers (Pe).

Peclet no. (Pe)	Order of Scheme-1	Order of Scheme-2
0.1	1.963	1.932
1	1.965	1.937
7	1.911	1.884
700	1.917	1.909

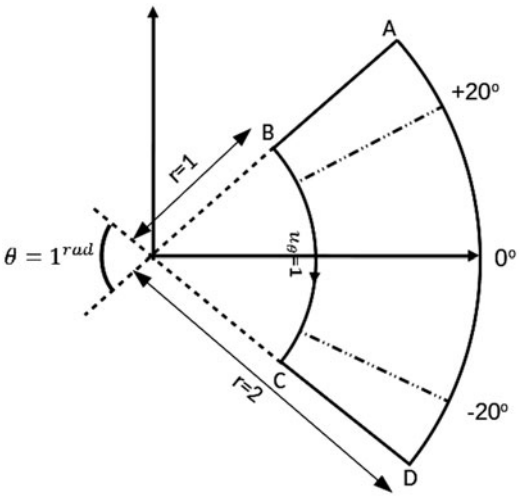

Figure 10. Polar-lid driven cavity with boundary conditions.

6.3. Test case-3

Finally Navier–Stokes equations are solved by the numerical scheme utilizing linear and quadratic elements (scheme-1) in arbitrary shaped domain. Polar lid-driven cavity is chosen as a test case to verify the applicability of this scheme in complex domain (Figure 10).

The physical domain for this polar lid driven cavity problem is shown in Figure 10. The angular size of domain is 1 *radian* and radial size is $1 \leq r \leq 2$.

In this 2D cylindrical wedge domain the boundary condition at BC surface $u_{1,\theta} = 1$. The boundary conditions on the other surfaces are no slip boundary conditions. Reynold number (Re) for the flow is defined using velocity of lid BC and radial width of domain.

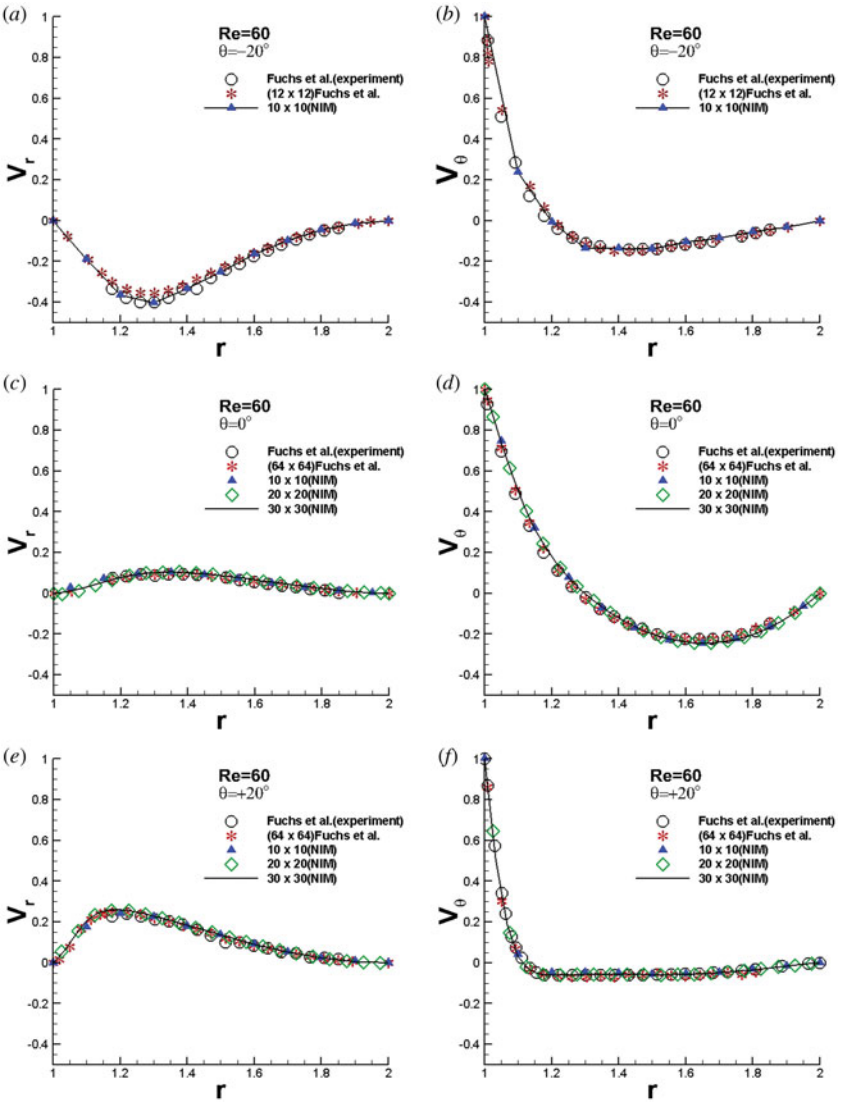

Figure 11. Comparison of velocity components at $\theta = -20^{\circ}, 0^{\circ}$ and 20°, for Re =60. (a) Radial component. (b) Angular component. (c) Radial component. (d) Angular component. (e) Radial velocity. (f) Angular component.

This problem definition of polar lid driven cavity is similar to the physical domain chosen by Fuchs and Tillmark [18]. For the comparative study, results are obtained for Re =60 and 350 using NIM scheme (scheme-1). Pressure correction based algorithm [9] is utilized for pressure velocity coupling. For both the Reynold numbers (Re =60 and 350), three different mesh sizes (10×10), (20×20) and (30×30) are chosen to generate the numerical results. Angular (V_θ) and radial (V_r) velocities are calculated at each surface of nodal cell using the numerical velocities (x and y components) available at the corresponding surfaces. These velocities (V_r and V_θ) are compared with the previously reported experimental and numerical results [18]. Results are compared at three different angles $-20^{\circ}, 0^{\circ}$ and $+20^{\circ}$ as shown in Figure 10.

Figure 11 is the plot of variation of the velocities in radial and angular directions at angles $-20^{\circ}, 0^{\circ}$ and $+20^{\circ}$ for Re =60. Figure 11(a) and 11(b) shows the velocity variations at -20°. In this figure, results obtained using coarsest grid size (10×10) by NIM scheme are compared with the results of Fuchs and Tillmark [18] using (12×12) grid size. This comparison is done with

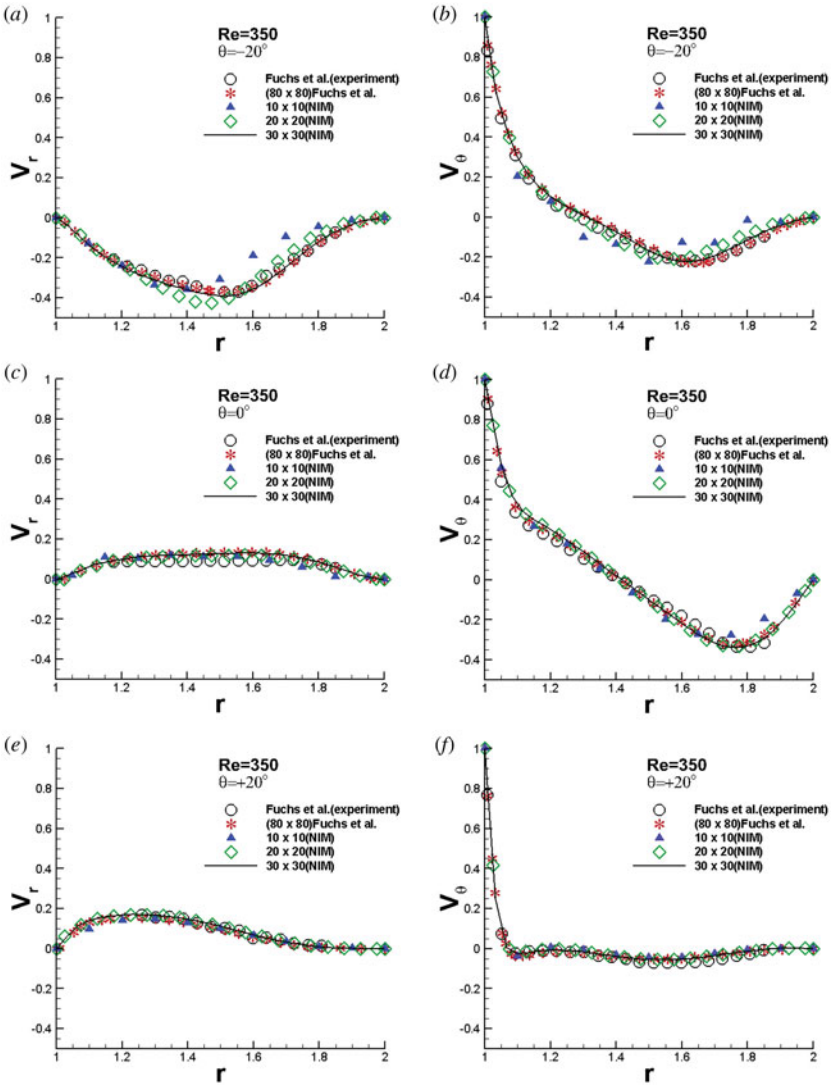

Figure 12. Comparison of velocity components at $-20^{\circ}, 0^{\circ}$ and 20° for Re $=350$. (a) Radial component. (b) Angular component. (c) Radial component. (d) Angular component. (e) Radial component. (f) Angular component.

reference to the experimental results [18]. It should be noted that the results of NIM based scheme for coarser grid size are much closer to the experimental results in comparison to the numerical results of Fuchs and Tillmark [18] for (12×12) grid sizes using multi-grid FDM. Figure 11(c) and 11(d) shows the variations of radial and angular velocities at an angle $\theta = 0^{\circ}$. Similarly the corresponding variations at an angle $\theta = +20^{\circ}$ are shown in Figure 11(e) and 11(f). The experimental and numerical results for grid size (64×64), reported by Fuchs and Tillmark [18], are also shown in this figure for comparison. It is observed from the plots that the results generated by NIM scheme even with quite coarse grid size of (10×10) are in good agreement with experimental and numerical results of Fuchs and Tillmark [18]. It is also noted that the results of different grid sizes using NIM methodology are quite close to each other.

In Figure 12 radial and angular velocities for Re $=350$ obtained by NIM are compared with experimental as well as numerical (80×80) results of Fuchs and Tillmark [18]. Again the

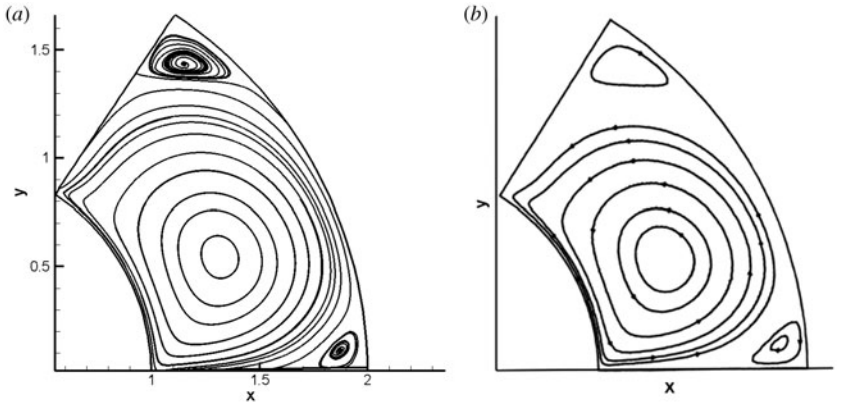

Figure 13. Stream lines contours at Re =350 by (a) NIM scheme-1 using (30×30) grid sizes (b) Fuchs and Tillmark [18] using (80×80) grid sizes.

comparison of the results are done on surfaces at $-20^{\circ}, 0^{\circ}$, and $+20^{\circ}$. Different mesh sizes (10×10), (20×20), and (30×30) are used by the NIM scheme for computation. It is observed that even the results obtained using quite coarse mesh size (10×10) is able to capture the flow physics, reported by Fuchs and Tillmark [18]. The comparison (Figure 12) shows that the velocity components at angles $\theta = 0^{\circ}$ and 20°, for all the grid sizes, agree fairly well with the fine mesh data of Fuchs and Tillmark [18] as shown in Figure 12(c,d) and 12(e,f). However, at -20° (Figure 12(a) and 12(b)) near the CD surface due to the formation of secondary small vortex (Figure 13), highly coarse grid of size (10×10) is not able to capture the physics properly.

Since the obtained numerical solutions, using NIM are cell averaged values thus there is more deviation between the fine grid solution [18] and results of NIM for (10×10) grid size. However, for grid sizes (20×20) and (30×30), the numerical results by NIM scheme are quite close to the experimental as well as fine mesh solution of Fuchs and Tillmark [18]. Figure 13 is the qualitative comparison of stream lines generated by NIM scheme (Figure 13(a)) and multi-grid finite difference method [18] (Figure 13(b)) for Re = 350. It is noted that the stream lines generated by NIM for grid size (30×30) are in good agreement with stream contours of Fuchs and Tillmark [18] using (80×80) grid size. Thus for this test case, fairly coarse grid size (30×30) results using the NIM scheme utilizing quadratic-linear quadrilateral elements is able to generate quite accurate results for Navier–Stokes equations in curvature domain.

7. Conclusions

A novel scheme for curved geometries using quadratic and linear quadrilateral elements by NIM is presented in this article. Both bi-quadratic and bi-linear Lagrange interpolation functions are used to map the corresponding quadratic and linear elements to square domains. Furthermore a novel approach is utilized to resolve the Neumann as well as mixed type boundary condition on the curved surfaces. In this approach the quadratic elements on the curved surface are piecewise linearized to implement both type of boundary conditions. The continuity conditions (C^1 type) at the interfaces of adjacent linear-linear, quadratic-linear cells and quadratic-quadratic cells are enforced. Current scheme is tested for both linear (Diffusion and Convection Diffusion) as well as non-linear equations (Navier–Stokes) in curved domain. For linear equations the numerical results are quite accurate with reference to analytical solutions even for quite coarse grid size. Currently developed scheme is able to resolved the Neumann boundary condition efficiently on the curved boundary. The scheme for convection diffusion equation retains its efficiency for both

low (Pe =7) and high (Pe =700) Peclet number. Also the comparative study between the scheme-1 (quadratic and linear quadrilateral elements) and scheme-2 (linear quadrilateral elements) reveals that scheme-1 is more accurate in comparison to scheme-2. Utilization of quadratic elements on curved boundary improves the accuracy of NIM scheme. Again the NIM scheme is tested for non-linear flow equations in polar lid driven cavity. The numerical results, obtained for Reynold number 60 and 350, are compared with experimental as well as fine mesh numerical results. The comparison shows that the developed NIM scheme is able to capture the flow physics with reasonable coarse grid size in curvature domain. Thus the developed numerical scheme utilizing quadratic and linear quadrilateral elements based on NIM methodology has retained its essence to solve the flow equations in complex domain with reasonably coarse grid size.

Acknowledgments

This research did not receive any specific grant from funding agencies in the public, commercial, or not-for-profit sectors.

References

[1] H. Fisher, and H. Finnemann, "The nodal integration method, a diverse solver for neutron diffusion problems," *Atomkernenergie Kerntechnik*, vol. 39, pp. 229–236, 1981.

[2] Y. Y. Azmy, and J. J. Dorning, *A Nodal Integral Approach to the Numerical Solution of Partial Differential Equation, Advances in Reactor Computations*, vol. 2, pp. 893–909. LaGrange Park IL: American Nuclear Society, 1983.

[3] Y. Y. Azmy, "A nodal integral method for the neutron diffusion equation in cylindrical geometry," *Trans. Am. Nucl. Soc.*, vol. 54, pp. 183–184, 1987.

[4] J. P. Hennart, "On the numerical analysis of analytical nodal methods," *Numer. Methods Partial Differ. Eq.*, vol. 4, no. 3, pp. 233–254, 1988.

[5] E. P. E. Michael, J. J. Dorning, and E. M. Gelbard, Rizwan-Uddin, "A nodal integral method for the convection-diffusion heat equation," *Trans. Am. Nucl. Soc.*, vol. 69, pp. 239–241, 1993. doi:10.13182/NSE137-380.

[6] Rizwan-Uddin, "A second-order space and time nodal method for the one-dimensional convection-diffusion," *Comput. Fluids*, vol. 26, pp. 233–247, 1997. doi:10.1016/S0045-7930(96)00039-4.

[7] F. Wang, "Rizwan-Uddin, a modified nodal scheme for the time dependent incompressible Navier-Stokes equations," *J. Comput. Phys.*, vol. 187, pp. 168–196, 2003. doi:10.1016/S0021-9991(03)00093-7.

[8] N. Kumar, S. Singh, and J. B. Doshi, "Nodal integral method using quadrilateral elements for transport equations: Part-1 convection-diffusion equation," *Numer. Heat Transf., Part B: Fund.*, vol. 64, no. 1, pp. 1–21, 2013. doi:10.1080/10407790.2013.784125.

[9] N. Kumar, S. Singh, and J. B. Doshi, "Pressure correction-based iterative scheme for Navier-Stokes equations using nodal integral method," *Numer. Heat Transf., Part B: Fund.*, vol. 62, no. 4, pp. 264–288, 2012. doi:10.1080/10407790.2012.709169.

[10] A. J. Toreja, "Rizwan-Uddin, hybrid numerical methods for convection-diffusion problems in arbitrary geometries," *Comput. Fluids*, vol. 32, pp. 835–872, 2003. doi:10.1016/S0045-7930(02)00031-2.

[11] W. Fitzpatrick, "Developments in nodal reactor analysis tools for hexagonal geometry," Ph.D. thesis, University of Illinois at Urbana-Champaign, Chicago, Illionis, 1995.

[12] Y. Hu, X. Zhao, and Q. Du, "A nodal green's function method for cylindrical geometry," Proceedings of International Conference on the Physics of Nuclear Science and Technology, LaGrange Park, IL: American Nuclear Society, pp. 799–802, 1998.

[13] S. T. Kim, and J. J. Dorning, "Discrete nodal and s-n transport methods for boundary-fitted coordinate geometries," Proceedings of the Topical Meeting on Advances in Nuclear Engineering Computation and Radiation Shielding, LaGrange Park, IL: American Nuclear Society, vol. 1, pp. 1–15, 1989.

[14] K. Huang, "Rizwan-Uddin, modified nodal integral method incorporated with irregular-shape-elements for Navier-Stokes equations, International Conference on Mathematics, Computational Methods & Reactor Physics (M&C 2009) Saratoga Springs, New York, May 3–7, 2009, LaGrange Park, IL: American Nuclear Society, 2009.

[15] O. G. Komlev, and I. R. Suslov, "A nodal expansion method for the neutron diffusion equation in cylindrical geometry," Proceedings of the International Conference on Mathematics and Computations, Reactor Physics, and Environmental Analyses, LaGrange Park, IL: American Nuclear Society, pp. 1428–1434, 1995.
[16] P. Wang, "Rizwan-Uddin, a modified, hybrid nodal-integral/finite-element method for 3d convection-diffusion problems in arbitrary geometries," *Int. J. Heat Mass Transf.*, vol. 122, pp. 99–116, 2018. doi:10.1016/j.ijheatmasstransfer.2018.01.087.
[17] E. G. Nezami, S. Singh, and N. Sobh, "Rizwan-Uddin, a nodal integral method for quadrilateral elements," *Int. J. Numer. Meth. Fluids*, vol. 61, pp. 144–164, 2009. doi:10.1002/fld.1949.
[18] L. Fuchs, and N. Tillmark, "Numerical and experimental study of driven flow in a polar cavity," *Int. J. Numer. Meth. Fluids*, vol. 5, no. 4, pp. 311–329, 1985. doi:10.1002/fld.1650050403.
[19] N. Kumar, S. Singh, and J. B. Doshi, "Nodal integral method using quadrilateral elements for transport equations: Part-2 Navier-Stokes equations," *Numer. Heat Transfer, Part B: Fund.*, vol. 64, no. 1, pp. 22–47, 2013. doi:10.1080/10407790.2013.784124.
[20] Rizwan-Uddin, "An improved coarse-mesh nodal integral method for partial differential equations," *Numer. Methods Partial Differ. Eqs.*, vol. 13, pp. 113–145, 1997. doi:10.1002/(SICI)1098-2426(199703)13:2¡113::AID-NUM1¿3.0.CO;2-S.
[21] Y. Y. Azmy, "Nodal method for fluid mechanics and neutron transport," Ph.D. thesis, University of Illinois Urbana-Champaign, Chicago, Illinois, 1985.
[22] W. Lilong, C. Bin, and Z. Gaoling, "An improved bubble packing method for unstructured mesh generation with applications in computational fluid dynamics," *Numer. Heat Transfer, Part B: Fund*, vol. 58, pp. 343–369, 2010. doi:10.1080/10407790.2010.511970.
[23] C. Shu, X. D. Niu, and Y. T. Chew, "Taylor series expansion and least squares-based lattice Boltzmann method: Three-dimensional formulation and its applications," *Int. J. Mod. Phys. C*, vol. 14, no. 07, pp. 925–944, 2003. doi:10.1142/S0129183103005133.
[24] Y. Wang, C. Shu, and C. J. Teo, "Development of lbgk and incompressible lbgk based lattice Boltzmann flux solvers for simulation of incompressible flows," *Int. J. Numer. Meth. Fluids*, vol. 75, no. 5, pp. 344–364, 2014. doi:10.1002/fld.3897.
[25] C. Ollivier-Gooch, and M. Van-Altena, "A high-order-accurate unstructured mesh finite-volume scheme for the advection-diffusion equation," *J. Comput. Phys.*, vol. 181, no. 2, pp. 729–752, 2002. doi:10.1006/jcph.2002.7159.

Appendix A

In Eq. (4) local coordinates (ξ, η) are considered as dependent variables. These dependent variables are function of independent variables x and y as one can solve the above Eq. (4) for x and y. On differentiating the Eq. (4) with respect to x:

$$1 = C_1\xi_x + C_2\eta_x + C_5(\eta_x\xi + \eta\xi_x) + 2C_3\xi\xi_x + 2C_4\eta\eta_x + C_6\left(2\xi\xi_x\eta + \xi^2\eta_x\right) + C_7\left(\xi_x\eta^2 + 2\xi\eta\eta_x\right) + C_8\left(2\xi\xi_x\eta^2 + 2\xi^2\eta\eta_x\right) \tag{A.1}$$

$$0 = D_1\xi_x + D_2\eta_x + D_5(\eta_x\xi + \eta\xi_x) + 2D_3\xi\xi_x + 2D_4\eta\eta_x + D_6\left(2\xi\xi_x\eta + \xi^2\eta_x\right) + D_7\left(\xi_x\eta^2 + 2\xi\eta\eta_x\right) + D_8\left(2\xi\xi_x\eta^2 + 2\xi^2\eta\eta_x\right) \tag{A.2}$$

Both the equations of Eqs. (A.1 and A.2) contains derivative of local variables ξ and η in terms of Cartesian coordinates of global cell which is valid for all quadratic elements. Similarly a set of equations is obtained from Eq. (4) when differentiating with respect to y.

$$1 = C_1\xi_y + C_2\eta_y + C_5\left(\eta_y\xi + \eta\xi_y\right) + 2C_3\xi\xi_y + 2C_4\eta\eta_y + C_6\left(2\xi\xi_y\eta + \xi^2\eta_y\right) + C_7\left(\xi_y\eta^2 + 2\xi\eta\eta_y\right) + C_8\left(2\xi\xi_y\eta^2 + 2\xi^2\eta\eta_y\right) \tag{A.3}$$

$$0 = D_1\xi_y + D_2\eta_y + D_5\left(\eta_y\xi + \eta\xi_y\right) + 2D_3\xi\xi_y + 2D_4\eta\eta_y + D_6\left(2\xi\xi_y\eta + \xi^2\eta_y\right) + D_7\left(\xi_y\eta^2 + 2\xi\eta\eta_y\right) + D_8\left(2\xi\xi_y\eta^2 + 2\xi^2\eta\eta_y\right) \tag{A.4}$$

Using these equations (Eqs. A.1–A.4), derivatives of local coordinates (ξ, η), ξ_x, ξ_y, η_x and η_y are evaluated as follows:

$$\mathbf{M}.\begin{bmatrix} \xi_x & \xi_y \\ \eta_x & \eta_y \end{bmatrix} = \begin{bmatrix} 1 & 0 \\ 0 & 1 \end{bmatrix} \tag{A.5}$$

or

$$\mathbf{J}(x,y)=\begin{bmatrix}\xi_x & \xi_y\\ \eta_x & \eta_y\end{bmatrix}=\begin{bmatrix}M_{11} & M_{12}\\ M_{21} & M_{22}\end{bmatrix}^{-1}=\mathbf{M}^{-1} \tag{A.6}$$

where the coefficients of **M** matrix are defined as:

$$\begin{aligned}M_{11}&=C_1+C_5\eta+2C_3\xi+2C_6\xi\eta+C_7\eta^2+2C_8\xi\eta^2\\ M_{12}&=C_2+C_5\xi+2C_4+C_6\xi^2+2C_7\xi\eta+2C_8\xi^2\eta\\ M_{21}&=D_1+D_5\eta+2D_3\xi+2D_6\xi\eta+D_7\eta^2+2D_8\xi\eta^2\\ M_{22}&=D_2+D_5\xi+2D_4+D_6\xi^2+2D_7\xi\eta+2D_8\xi^2\eta\end{aligned} \tag{A.7}$$

Similarly second order derivatives, $\xi_{xx},\xi_{yy},\eta_{xx}$, and η_{yy} are obtained. Again two sets of equations are obtained by differentiating Eqs. (A.1, A.2) with respect to x and Eqs. (A.3, A.4) with respect to y. These four equations (a set for x and another for y) are used to evaluate the second order derivatives for each cell by following the above mentioned procedure for first order derivatives.

The final form of coefficients of **H** matrix for second order derivatives $\xi_{xx},\xi_{yy},\eta xx$ and η_{yy} in Eq. (10) is:

$$\begin{aligned}H_{11}&=(C_5+2C_6\xi+2C_7\eta+4C_8\xi\eta)\xi_x\eta_x+\left(C_3+C_6\eta+C_8\eta^2\right)\xi_x^2+\left(C_4+C_7\xi+C_8\xi^2\right)\eta_x^2\\ H_{12}&=(C_5+2C_6\xi+2C_7\eta+4C_8\xi\eta)\xi_y\eta_y+\left(C_3+C_6\eta+C_8\eta^2\right)\xi_y^2+\left(C_4+C_7\xi+C_8\xi^2\right)\eta_y^2\\ H_{21}&=(D_5+2D_6\xi+2D_7\eta+4C_8\xi\eta)\xi_x\eta_x+\left(D_3+D_6\eta+D_8\eta^2\right)\xi_x^2+\left(D_4+D_7\xi+D_8\xi^2\right)\eta_x^2\\ H_{22}&=(D_5+2D_6\xi+2D_7\eta+4D_8\xi\eta)\xi_y\eta_y+\left(D_3+D_6\eta+D_8\eta^2\right)\xi_y^2+\left(D_4+D_7\xi+D_8\xi^2\right)\eta_y^2\end{aligned} \tag{A.8}$$

Appendix B

Coefficients of Eq. (26) are:

$$\begin{aligned}A_1&=\frac{Sm3_{(i,j)}}{2}\left\{\frac{Peu_{(i,j)}.e^{Peu_{(i,j)}}}{2.\left(1-e^{Peu_{(i,j)}}\right)}\right\}\\ A_2&=\frac{Sm1_{(i+1,j)}}{2}\left\{\frac{Peu_{(i+1,j)}.e^{Peu_{(i+1,j)}}}{2.\left(e^{Peu_{(i+1,j)}}-1\right)}\right\}\\ A_3&=\frac{2.Sm3_{(i,j)}}{\alpha_{\xi(i,j)}}\left\{\frac{1}{Peu_{(i,j)}}-\frac{e^{Peu_{(i,j)}}}{1-e^{-Peu_{(i,j)}}}\right\}\\ A_4&=\frac{2.Sm1_{(i+1,j)}}{\alpha_{\xi(i+1,j)}}\left\{\frac{e^{Peu_{(i+1,j)}}}{1-e^{-Peu_{(i+1,j)}}}-\frac{1}{Peu_{(i+1,j)}}\right\}\end{aligned} \tag{B.1}$$

Similarly coefficients of three point scheme B_i in η direction are obtained.